


Self-growing protocell models in aqueous two-phase system induced by internal DNA replication reaction

Received: 9 September 2024

Accepted: 10 January 2025

Published online: 26 February 2025

Yoshihiro Minagawa^{1,4}, Moe Yabuta^{1,4}, Masayuki Su'etsugu² & Hiroyuki Noji^{1,3} 

The bottom-up reconstitution of self-growing artificial cells is a critical milestone toward realizing autonomy and evolvability. However, building artificial cells that exhibit self-growth coupled with internal replication of gene-encoding DNA has not been achieved yet. Here, we report self-growing artificial cell models based on dextran-rich droplets in an aqueous two-phase system of poly(ethylene glycol) (PEG) and dextran (DEX). Motivated by the finding that DNA induces the generation of DEX-rich droplets, we integrate DNA amplification system with DEX-rich droplets, which exhibited active self-growth. We implement the protocells with cell-free transcription-translation systems coupled with DNA amplification/replication, which also show active self-growth. Considering the simplicities in terms of the chemical composition and the mechanism, these results underscore the potential of DEX droplets as a foundational platform for engineering protocells, giving implications for the emergence of protocells under prebiotic conditions.

The bottom-up reconstitution of autonomous artificial cell systems from natural and/or synthetic components is one of the grand challenges in synthetic biology. Artificial cell models with essential features of living cells, such as replication of genetic materials, gene expression, information/energy transductions, and vesicle fission/division, have been developed to elucidate the working mechanism of molecular systems^{1–4}. The bottom-up approach of autonomous artificial cell systems also provides implications for possible scenarios on how protocells have emerged in prebiotic conditions⁵. From the engineering point of view, the open nature of artificial cell systems holds a great promise for technological innovations in the rapid prototyping or high-throughput screening of functional biomolecules/biosystems that would be applicable in various fields such as bioanalysis, medicine, and material science^{6–10}.

Autonomous artificial cell models should contain a genetic information-carrying molecule and a set of catalyst molecules that replicate genetic molecules and produce the catalyst molecules themselves. In addition, genetic molecules and catalyst molecules

should be micro-compartmentalized in a microreactor as a “cell” to define the identity of the cell and protect itself from inevitably emerging parasites¹¹. Considerable progress has been made in the reconstitutions of individual subcellular systems such as DNA/RNA amplification/replication, coupled transcription and translation (TXTL), lipid synthesis, and lipid vesicle division machinery^{12–18}. However, there are still large gaps between natural and artificial cells in terms of the orchestration of multiple functions to realize autonomy. In particular, the growth and division of micro-compartmentalizing vesicles or reactors coupled with the replication of genetic materials remain as a grand challenge.

Membrane vesicles composed of fatty acids or phospholipids are the gold standard for the micro-compartmentalization in artificial cell research. Dynamic morphological changes in vesicles, such as growth, fission, and division, were observed when fatty acids or lipids were externally or enzymatically supplied or when the excluded volume effect of DNA was applied to the lumen of the vesicle^{14,19–24}. Some studies have tried to achieve vesicle self-growth coupled with internal

¹Department of Applied Chemistry, School of Engineering, The University of Tokyo, Tokyo, Japan. ²Department of Life Science, College of Science, Rikkyo University, Tokyo, Japan. ³UT7 Next Life Research Group, The University of Tokyo, Tokyo, Japan. ⁴These authors contributed equally: Yoshihiro Minagawa, Moe Yabuta. ✉ e-mail: hnoji@g.ecc.u-tokyo.ac.jp

gene expression, but no significant membrane or volume expansion was observed^{14,17,25}. In addition, autonomously self-growing vesicles with gene amplification have not yet been developed.

Another class of micro-compartmentalization methods that have recently attracted growing attention is liquid–liquid phase separation (LLPS)^{2,4,26}. Microdroplets formed via LLPS have no physical boundary between droplets and external continuous phase, thus enabling solute exchange with the continuous phase and allowing a continuous supply of substrate molecules, such as nucleic acids and amino acids, from the external solution. In addition, some types of LLPS droplets can enrich the biopolymers inside them. Taking these advantageous features, various studies were reported to attempt to construct artificial cell models. In particular, coacervates were often used^{4,27}. Although several studies have reported that the growth of coacervate droplets by producing constituting molecules of coacervates^{28–30}, the self-growing protocell models that couple the gene replication have not been achieved yet.

In contrast, aqueous two-phase system (ATPS) has two solution constituents, in which polymers become immiscible at over-threshold concentrations. The ATPS of dextran (DEX) and poly(ethylene glycol) (PEG) is one of the best characterized. It is currently attracting great interest because the DEX-rich phase preferentially enriches nucleic acid polymers, such as DNA and RNA, as well as some types of folded proteins^{31–35}. The *in vitro* TXTL within the DEX-rich droplets in PEG/DEX ATPS have also been reported³⁶. Thus, PEG/DEX ATPS system has been recognized as an alternative to liposomes or coacervate droplets for the generation of artificial cell models.

In this study, we first investigated the interplay between PEG/DEX ATPS and DNA. Then, we constructed DEX droplet-based artificial cell models that exhibit autonomous growth coupled with internal DNA replication or RNA production. We also tested the artificial cell model of DEX-rich droplets that undergo TXTL-coupled DNA amplification/replication to drive the active growth.

Results

We used DEX (MW: 550 kDa) and PEG (MW: 35 kDa) in this study. The composition of the PEG/DEX mixture is presented as a coordinate for simplicity; for example, (4.0, 4.0) means a mixture of 4.0 w/w% DEX and 4.0 w/w% PEG. First, we quantitatively measured the partitioning ratio of dsDNA in the DEX-rich phase of the PEG/DEX ATPS (4.0, 4.0) (Fig. 1a) from the fluorescence signal of SYBR Gold according to calibration curves (Supplementary Fig. 1). Linear DNAs with lengths of 10 bp, 100 bp, and plasmid DNAs with 4×10^3 , or 2×10^5 bp were tested. The partitioning ratio of DNA in the DEX-rich phase increased with DNA length (Fig. 1b). 4 and 205 kbp DNAs were almost exclusively enriched in the DEX phase, whereas the 10 bp DNA was evenly partitioned in the DEX-rich and PEG-rich phases.

Then, we examined whether DNA induces phase separation of the PEG/DEX system by comparing phase transition of PEG/DEX systems with or without DNA of 4 or 205 kbp at 950 ng/ μ L. We employed titration experiment³⁷, where PEG/DEX ATPS solution was iteratively diluted by pure water to determine the point at which ATPS turned to a miscible solution. Figure 2a shows a representative result of titration experiment starting from (2.3, 2.3). Upon dilution, the PEG/DEX ATPS without DNA became miscible at first, whereas the solution with DNA still exhibited phase separation. With continuous dilution, the solution with 4 kbp DNA became a single phase while the solution with 205 kbp DNA remained in a two-phase state. Further dilution eventually resulted in the phase transition of the solution with 205 kbp DNA. This result shows that DNA stabilizes PEG/DEX ATPS. The titration experiment was repeated three times for each condition to determine the probability of the phase transition (Fig. 2b) because phase transition stochastically occurred around the threshold concentration. This is attributable to the subtle differences in experimental conditions

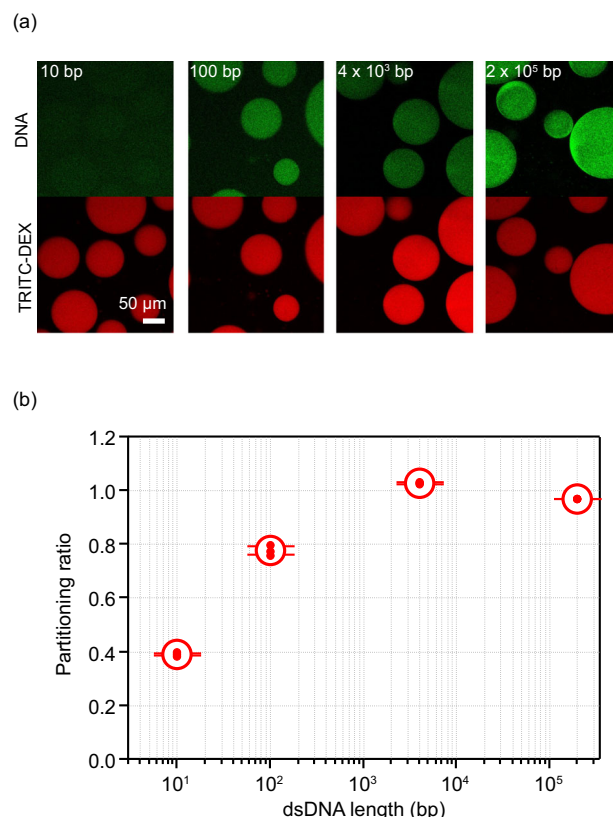


Fig. 1 | DNA partitioning in PEG/DEX ATPS. a Confocal fluorescence images of DNA stained with SYBR Gold in (4.0, 4.0) PEG/DEX mix (i.e., 4.0 w/w% DEX and 4.0 w/w% PEG). Concentrations are expressed as coordinates. **b** Partitioning ratio of DNA between the DEX-rich and PEG-rich phases. 10 bp, 100 bp, 4 kbp, and 205 kbp double-stranded DNAs were presented as mean \pm SD ($n = 3$). The values are as follows: 205 kbp, 0.97 ± 0.00012 ; 4 kbp, 1.0 ± 0.0030 ; 100 bp, 0.78 ± 0.016 ; and 10 bp, 0.39 ± 0.0057 .

and/or the intrinsic stochasticity of PEG/DEX phase transition. We determined the point for a 50% probability of phase transition as the critical concentration for the phase transition, by fitting the data points with a hyperbolic tangent function. We conducted titration experiments starting from six different compositions (Supplementary Fig. 2) to draw the binodal curves in the phase diagram (Fig. 2c), which clearly showed that DNA stabilizes PEG/DEX ATPS. In particular, 205 kbp DNA showed a significant effect on the stabilization of phase separation.

The results of the titration experiments suggest the possibility that DNA amplification can induce the formation of DEX-rich droplets from miscible PEG/DEX solutions. To test this idea, we microscopically observed the PEG/DEX solution in the presence of a DNA amplification reaction mix. The initial PEG/DEX concentrations were set at (2.00, 2.00) which is between the binodal curves w/4 kbp DNA or w/o DNA as indicated by the crosspoint of dash lines in Fig. 2c: (2.09, 2.09) for w/o DNA and (1.95, 1.95) for w/4 kbp DNA. The reaction mixture of rolling circle amplification (RCA) with EquiPhi29 DNA polymerase was added to the PEG/DEX mix with circular template DNA of 205 kbp at 8 pM (1 ng/ μ L) (Fig. 3a). In this study, EquiPhi29 DNA polymerase (EquiPhi29DNAP)³⁸, an activity-enhanced mutant of Phi29 DNA polymerase was used in RCA throughout the experiments. Note that the initial template DNA concentration was too low to induce spontaneous phase separation. The PEG/DEX mixture was introduced into a flow cell chamber and observed under a fluorescence microscope. After incubation at 33 °C for 16 h, many DEX-rich droplets with the diameter up to 40 μ m appeared (Fig. 3b). Hereafter, DEX-rich droplet is referred to as DEX droplet for simplicity. All DEX droplets enriched DNA inside.

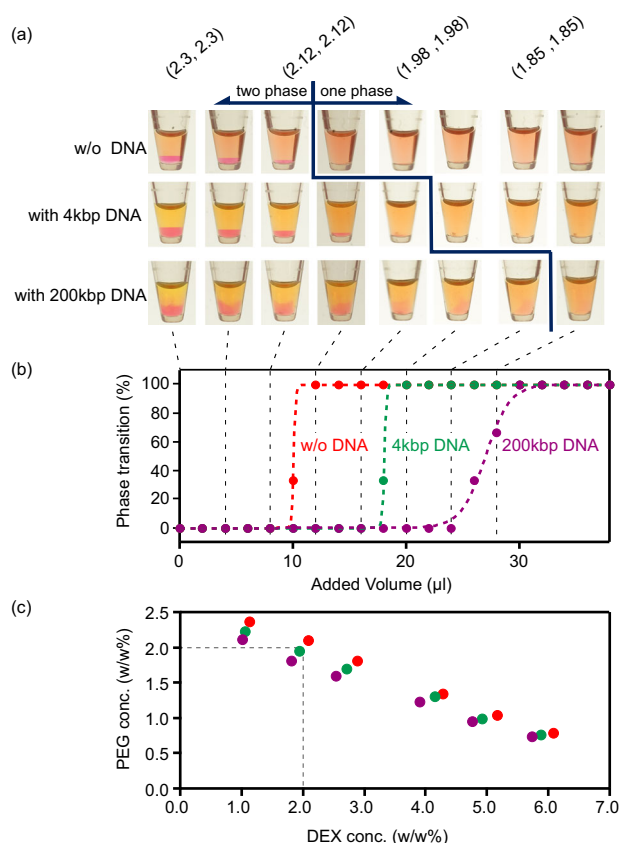


Fig. 2 | Titrimetry of PEG/DEX ATPS with or without DNA. a Photos of the titration experiment of PEG/DEX ATPS with DNA. PEG/DEX mix of (2.3, 2.3) was serially diluted by adding small amount of pure water (for details, see “Methods”). The upper brackets indicate PEG/DEX compositions during titration. The PEG-rich layer (top layer in a tube) and the DEX-rich layer (bottom layer in a tube) were stained with TRITC-DEX and FITC-PEG, respectively. **b** Probabilities of phase transition determined from three independent experiments. The data points were fitted on hyperbolic tangent functions to determine the critical concentrations (Supplementary Fig. 2). **c** The critical concentrations for the phase transition in the absence or presence of DNA: red, without DNA; green, with 4 kbp DNA; purple, with 205 kbp DNA. The crosspoint of dashed lines indicates (2.0, 2.0) which lies between the critical concentrations with 4 kbp DNA and without DNA. This condition was employed in the following experiments for ATPS induction.

When PEG or DEX was absent in the solution, droplets were not observed (Supplementary Fig. 3). DEX droplet generation was also observed when 12 kbp DNA was used as template DNA. In both experiments, time-lapse images showed that DEX droplets appeared and actively coalesced with other droplets (Supplementary Video 1). These observations demonstrated that DNA amplification induces the phase separation of PEG/DEX solution and the growth of DEX droplets.

For quantitative analysis on the active growth of DEX droplets, we conducted time-lapse observation of DEX droplets (Fig. 4a). DEX droplets in PEG/DEX ATPS solution were prepared and preloaded with RCA reaction mixture containing template 4.2 kbp circular DNA. After being introduced into a flow cell, DEX droplets spontaneously settled out due to higher density compared to PEG-rich solution, and stably attached to the coverslip, allowing for time-lapse imaging. While the initial size of DEX droplet differed in each preparation, the diameter ranged typically from 4 to 15 μm with the volume from 30 to 1800 fL (Supplementary Fig. 4a). Upon the incubation at 30 °C, the droplets showed active growth (Fig. 4b and Supplementary Video 2). Droplets showed clear volume expansion; most of the droplets increased the volume 2-fold and some showed over 7-fold expansion (Fig. 4c). After 200 min, most of droplets reached a plateau size pausing the growth,

probably due to the complex nature of RCA; RCA yields dendritic DNA clusters as the reaction product, hampering further DNA amplification. We observed moderate tendency that smaller droplets were more active for volume expansion (Supplementary Fig. 4b). When Equiφ29DNAP was not added, droplets did not show the obvious growth, confirming the active growth was driven by DNA amplification (Supplementary Fig. 5). Note that small aggregates were formed on the surface of DEX droplets for unknown reasons in the presence of fluorescently labeled DEX (TRITC-DEX) at 0.05 w/w%. Therefore, TRITC-DEX was added at 0.01 w/w% in the following experiments.

We also monitored DNA concentration inside the droplets by staining with SYTO 12 (Fig. 4d, Supplementary Video 3 and Supplementary Figs. 6 and 7). Figure 4e shows representative time-courses of [DNA] and the droplet volume. While [DNA] increased along with the droplet growth, [DNA] reached a plateau level even earlier than droplet growth. This trend was observed for other droplets (Supplementary Fig. 7). Interestingly, the plateau levels of [DNA] were found around 2000 ng/μL. This suggests that 2000 ng/μL is close to the upper limit for DEX droplets to accommodate DNA inside under the present condition. When the rate of volume expansion was plotted against [DNA], it turned out that the growth rate monotonically increased with [DNA] until reaching the plateau level (Fig. 4f). Considering that the rate of DNA amplification should increase in proportion to [DNA] in the early phase, it is reasonable to observe that the droplet growth is highly dependent on the internal [DNA] when it is below the upper limit.

For the further confirmation that internal DNA amplification directly drives the droplet growth, we tested the reverse reaction by adding DNase I to the grown droplets (Supplementary Fig. 8a and Supplementary Video 4). As expected, the droplets exhibited evident shrinkage with DNA degradation (Supplementary Fig. 8b). After the fluorescence of SYTO 12 dropped almost to the background level, the shrinkage ceased. The final volume of the droplets was approximately the half of the droplet volume when DNase treatment was initiated. In this condition, the RCA induced the volume expansion for around 4-fold in average. Thus, the shrinkage stopped when the volume dropped at the 2-fold of the initial volume before RCA-induced growth. The modest shrinkage is reasonable because the PEG/DEX solution was almost on the bimodal curve where the system was in quasi-equilibrium condition. These observations confirmed the growth mechanism; DNA amplification directly drives the growth of the DEX droplet, stabilizing the ATPS.

We then asked whether RNA was also able to induce phase separation in the PEG/DEX system. When RNA with 1.75×10^3 nt in length at 623 ng/μL was spiked to PEG/DEX mix at (2.0, 2.0), the PEG/DEX mix underwent phase separation, generating DEX droplets (Fig. 5a, b). We also confirmed that in vitro transcription in miscible PEG/DEX mix induces phase separation (Fig. 5c, d). Thus, it was confirmed that in situ RNA production can also induce the phase separation of PEG/DEX solution as well as DNA amplification.

To seek more autonomy of the DEX droplet as the artificial cell model, cell-free transcription-translation system (TXTL) was added with the template DNA encoding Equiφ29DNAP to implement TXTL-coupled RCA system in the DEX droplets (Fig. 6a)³⁹. We prepared PEG/DEX ATPS mix containing the cell-free TXTL system from purified components, PURE system⁴⁰. While most of PURE system components such as ribosome, transcription factors are intrinsically enriched in the DEX-rich phase³⁶, Equiφ29DNAP is almost evenly partitioned in both DEX-rich and PEG-rich phases. In order to retain expressed Equiφ29DNAP inside the droplet, it was tagged with dextran binding domain (DBD) by genetic fusion⁴¹. The growth activity of the DEX droplets was investigated in time-lapse imaging with confocal microscope. Many of droplets showed continuous growth over 720 min (Fig. 6b, c and Supplementary Video 5). The growth rate was slower than that of droplets carrying purified RCA components, probably due

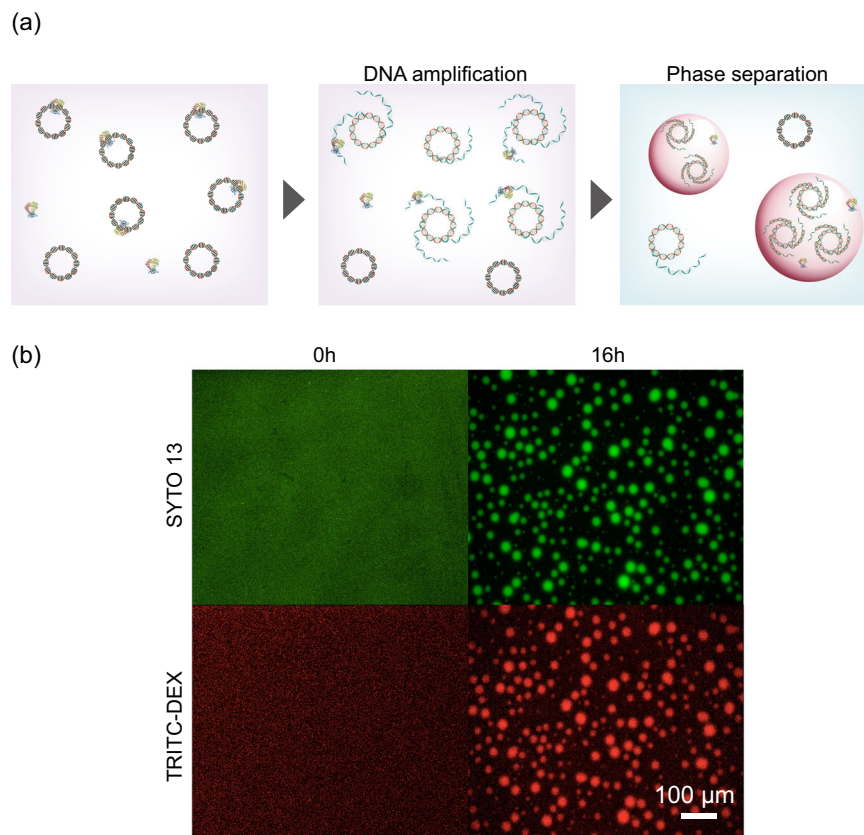


Fig. 3 | Phase separation induced by RCA. a Experimental diagram of phase separation induced by RCA. RCA was conducted with ϕ 29 DNA polymerase in miscible PEG/DEX mix (2.00, 2.00). The image of ϕ 29 DNA polymerase is obtained from PDB (PDB ID: 1XHX). **b** Fluorescence images show the reaction at the start (0 h,

left) and at 16 h (right). DNA and DEX were stained with SYTO 13 (green, top) and TRITC-DEX (red, bottom). Experiments were repeated more than three times with similar results.

to the cascade reaction of TXTL-coupled RCA. Many of droplets increased the volume over 3-fold during 12 h incubation, and some were significantly active in the growth, expanding the volume over 10-fold (Fig. 6d and Supplementary Fig 9a, b). When dNTPs were omitted, droplets did not show obvious growth, confirming that DNA amplification plays a most significant role in the growth among the transcription, translation, and DNA amplification (Supplementary Fig. 10).

Then, we attempted to implement a recursive DNA replication system that produce the exact same copies of template DNA in terms of length and topology. Of isothermal and recursive DNA replication systems^{12,42,43}, we employed the reconstituted ϕ 29 phage genome replication system, terminal protein primed DNA amplification (TPPDA)⁴², considering the simplicity and the application for a protocell model⁴⁴. TPPDA is principally composed of four components: terminal protein (TP), DNA polymerase (ϕ 29 DNA polymerase), ssDNA binding protein (SSB), dsDNA binding protein (DSB). Prior to the growth experiment under microscope, we confirmed that TXTL-coupled TPPDA system retains the functionality to replicate DNA in PEG/DEX ATPS (Supplementary Fig. 11). To implement TXTL-coupled TPPDA system in the DEX droplet, 13 kbp linear DNA encoding genes of TP and ϕ 29 DNA polymerase was added as the template DNA, while SSB and DSB were added as purified proteins with PURE system (Fig. 7a). The DEX droplets implemented with TXTL-coupled TPPDA showed continuous self-growth activity over 280 min and exhibited volume expansion: 1.8 ± 0.2 -fold (Fig. 7b–d, Supplementary Fig. 12a, b, and Supplementary Video 6). When dNTPs were omitted, the droplets did not show the obvious growth, indicating that DNA replication is the primary factor driving growth. (Supplementary Fig. 13). Thus, the DEX droplet-based protocell model showed self-growth activity to increase the volume

almost two times upon the recursive DNA amplification. The growth activity is moderate in comparison with the growth activity by TXTL-coupled RCA. This is attributable to the complex nature of TPPDA; this recursive replication system requires four protein components while RCA requires only polymerase, and thereby TPPDA should be more susceptible to the leakage effect and the interaction with PEG/DEX. In particular, we noticed that TP-attached DNA products are prone to form aggregation (Supplementary Fig. 14), that would at least partially explain the lower activity of TPPDA-driven self-growth.

Discussion

The PEG/DEX system is one of the best-characterized aqueous phase separation systems. Preferential partitioning of biopolymers, such as DNA, RNA, proteins, and protein filaments, in the DEX-rich phase has been reported^{31–35}. However, the reverse effect, that is, phase stabilization by such biopolymers, has not been reported. This study showed that DNA stabilizes the ATPS of the PEG/DEX system and quantitatively analyzed the impact of DNA on the phase separation. We also found RNA induces phase separation although the quantitative analysis was not allowed due to the difficulty of large-scale preparation of homogeneous RNA sample. The stabilization effect of DNA was observed in narrow conditions; (2.09, 2.09)–(1.81, 1.81) for 205 kbp DNA when the titration experiment started from (2.30, 2.30). In addition, a large quantity of DNA or RNA (600–900 ng/ μ L) was required to observe the stabilization of ATPS. These might be the reason why the stabilization effect of the DNA/RNA reverse effect has not been found in previous works.

Longer DNA stabilized ATPS more efficiently. This is in accordance with the trend of the partitioning ratio in the DEX-rich phase,

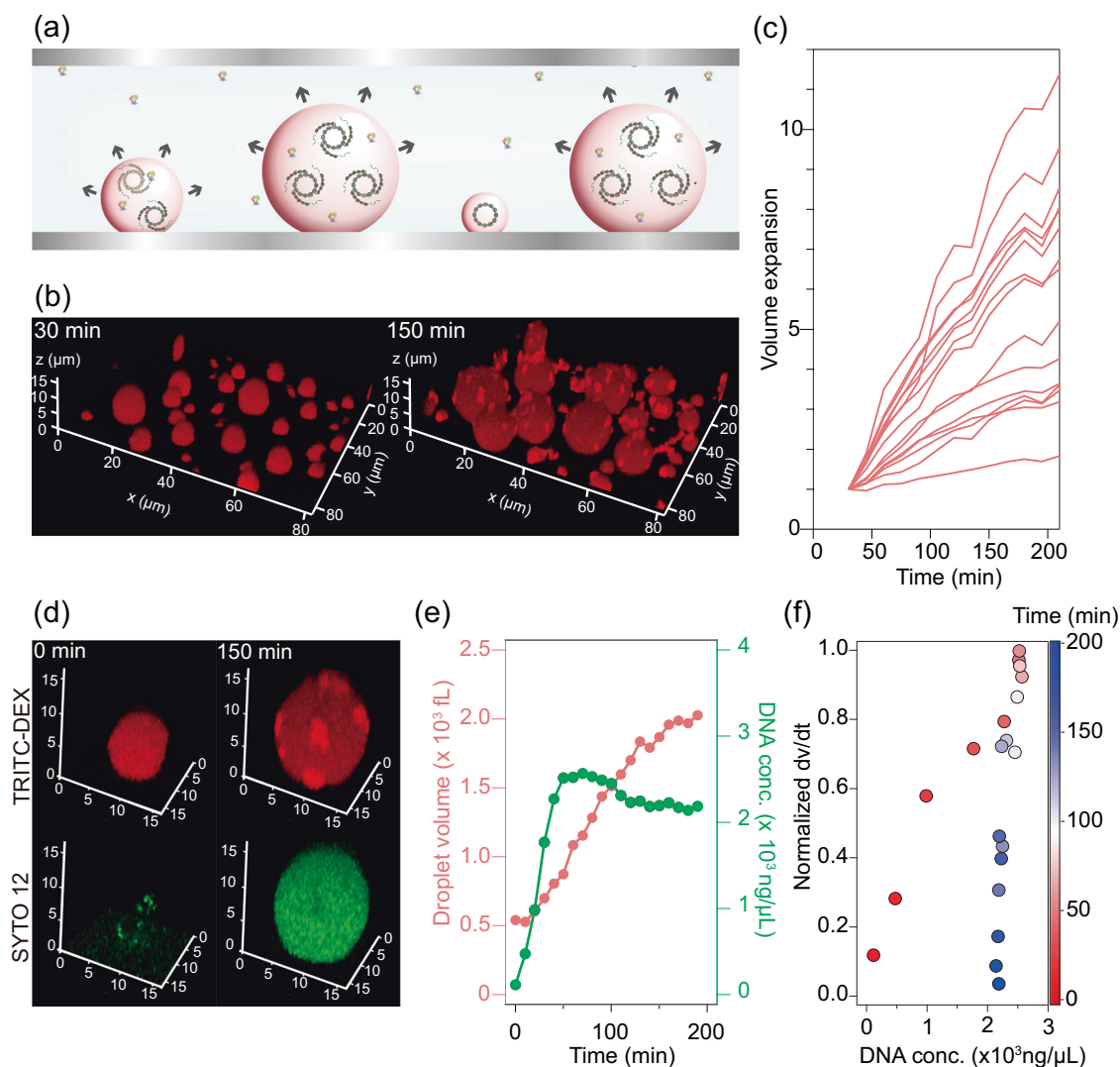


Fig. 4 | Self-growth induced by RCA. **a** Schematic image of DEX droplets self-growth induced by DNA amplification. DNA is amplified by RCA catalyzed by Equi ϕ 29DNAP. The image of phi29 DNA polymerase is obtained from PDB (PDB ID: 1XHX). **b** Confocal images of the protocell stained with TRITC-DEX (red). Fluorescence images show the reaction at 30 min (left) and at 150 min (right). **c** Time-courses of the volume of DEX droplets. The first 30 min was omitted because small droplets occasionally coalesced to other droplets in the first 30 min. The volume was normalized with that at 30 min and plotted. **d** Magnified images of DEX

droplets stained with TRITC-DEX (red) and with SYTO 12 (green) at 0 min (left) and at 150 min (right). **e** Time-course of the volume changes and DNA concentration of the droplet shown in (d). Time-courses of other droplets are shown in Supplementary Fig. 7. **f** The normalized growth rate versus DNA concentration analyzed from the time-course in (e). The color of data points represents the incubation time, as shown in the color bar. Analyses for other droplets are also shown in Supplementary Fig. 7. Experiments of (b, d) were repeated three times with similar results, respectively.

suggesting that stabilization and partitioning are based on a common mechanism. DEX and PEG are chemically inert polymers without charged or aromatic rings, unlike droplet-forming biopolymers. Therefore, the interplay between DNA and the DEX-rich phase would be based on physicochemical principles rather than chemically specific interactions. Yoshikawa et al. have proposed that filamentous polymers/assemblies, such as double-stranded DNA and actin filaments, are more readily accommodated in larger void interspaces in the DEX-rich phase than in the PEG-rich phase³³. On the other hand, the present study found that RNA, a more flexible polymer is also preferentially enriched in the DEX phase, implying that other mechanisms might also exist.

One may ask that DNA or RNA contributes to the growth of DEX droplet as the droplet composition rather than the enhancer of the phase separation, considering that these nucleic acids have a sugar group as DEX. Although this is very intriguing; it would not be feasible for the following reasons. First, as shown in Fig. 4e, the growth rate of

DEX droplet was not well parallel to that of DNA amplification; DEX growth often showed the apparent lag time after the initiation of DNA amplification (Supplementary Fig. 8). The maximum growth rate was observed only when DNA concentration reached the plateau level. Another line of observation also supports this view; the DEX concentration was kept constant during the active droplet growth, suggesting the active uptake of DEX molecule from solution. Thus, these observations suggest that the main function of DNA/RNA for the droplet growth is the enhancer of the phase transition rather than the droplet composition.

By exploiting the phase stabilization effect of DNA, we developed self-growing protocell models. We implemented internal DNA/RNA synthesis reactions within DEX droplets. When RCA system was implemented, the DEX droplets showed significant growth of the droplet size, expanding the volume by 2–10 times. Simultaneous observation of the DNA amplification and droplet growth showed that the growth rate raised with the internal [DNA], and it reached the

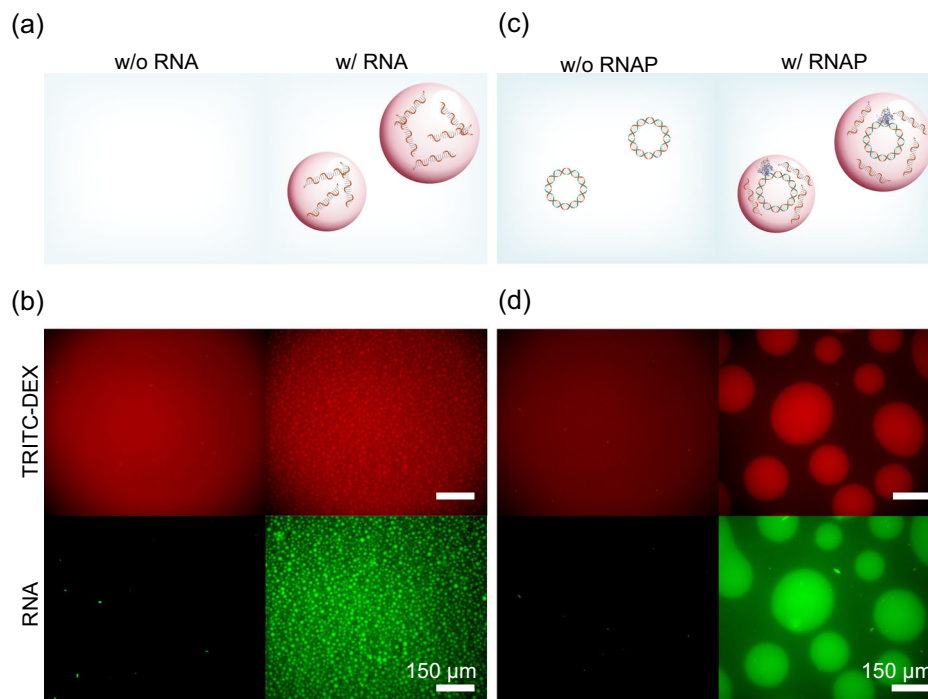


Fig. 5 | Phase separation induced by RNA. **a** Experimental diagram of **(b)**. **b** Phase separation induced by spiked RNA. Purified RNA was not added (left) or added to (2.00, 2.00) PEG/DEX system at 623 ng/μL. Fluorescence images were obtained by staining RNA containing Pepper sequence with HBC (green) and DEX with TRITC-DEX (red). **c** Experimental diagram of **(d)**. The image of T7 RNA polymerase is obtained from PDB (PDB ID: 1CEZ). **d** Phase separation induced by in situ RNA

transcription. Miscible PEG/DEX mix at (2.00, 2.00) containing 600 ng/μL template DNA was incubated with in vitro transcription system without (left) or with RNA polymerase (right). Fluorescence images were obtained by staining RNA containing Pepper sequence with HBC (green) and DEX with TRITC-DEX (red). Experiments of **(b)**, **(d)** were repeated three times with similar results, respectively.

maximum when [DNA] reached the plateau level around 2000 ng/μL. These observations showed that the internal DNA concentration acts as the internal pressure to drive the droplet growth.

In pursuit of a more autonomous protocell model, we attempted to implement the ability to self-producing enzymes for gene replication. At first, we implemented cell-free TXTL-coupled RCA. Upon the gene expression, the template DNA was amplified by the in situ produced *Equi*φ29DNAP that resultantly induced the active growth, achieving the growth ratio by 3–10 times. Then, we implemented cell-free TXTL-coupled recursive DNA replication system, TPPDA into DEX droplet. The DEX-droplets showed active growth over 280 min, expanding 1.8 times from the initial volume. Thus, we achieved the development of protocell models that undergo self-growth driven by internal amplification/replication of polymerase-encoding DNA coupled with gene expression.

There are other reports on self-growth activity of several protocell models. Liposome growth induced by in situ synthesis of lipid molecule catalyzed by chemical catalysts was actively studied^{14,45}. It was also attempted to build self-growing liposome systems with cell-free TXTL systems to produce enzymes for lipid synthesis^{14,17}. Although this strategy is the straightforward for build-a-cell, the visible growth was not observed, and not coupled with gene replication. The growth of peptide vesicles coupled with a gene expression system was reported⁴⁶. This system relied on an imbalance in osmotic pressure generated by transcripts or expressed proteins. Although growth coupled with TXTL system was achieved, growth coupled with gene replication has not yet been accomplished. The growth of coacervate droplets was also reported in several studies in which the growth was induced by the addition or enzymatic production of inducer chemicals such as ATP or UDP²⁹. However, the implementation of gene replication systems to induce self-growth of coacervate has remained challenging. DEX-droplet-based protocell models represent a completely new model with large potential to create protocells with autonomy;

because the driving force for self-growing is based on simple mechanism, the enzymes for the self-growing are genetically encodable and the genetic materials such as DNA and RNA are readily retained inside of the cells. Considering these points, the present study opens a new venue to build protocell models with high autonomy and functionality.

However, it should also be mentioned that there are many critical challenges for DEX-droplet-based protocell models. One major obstacle is how to implement the capability for self-division. Although the surface tension of DEX droplet is lower than that of water-in-oil droplet³³, it is still challenging to implement a mechanism to induce division of DEX droplets. In this regard, an implicative work was reported by Takinoue group⁴⁷. They have created oligo DNA droplet composed of modestly associating oligo DNA strands and succeeded in splitting droplets into two parts by introducing a restriction enzyme. Although the implementation of gene expression and gene replication are remaining challenges for their strategy, this work is very suggestive for the consideration of the division mechanism for DEX droplet-based protocell. Symmetry-breaking structures in DEX droplets would be a key factor.

The results of this study also provide valuable insights into how protocells could have arisen in environments prior to the emergence of primitive cells. While the protocell model used in this study is based on polymers that did not exist in prebiotic conditions, the self-growth mechanism discovered here highlights the reverse reaction of preferential partitioning of solute molecules that, in turn, induce and stabilize phase separation. This could be a phenomenon universally observed in other phase-separating systems, including those that might have existed on primitive Earth. The self-growth mechanism demonstrated in this study is much simpler and more easily coupled with gene replication compared to liposome-based protocells. The simplicity of the self-renewal mechanism in DEX droplet-based protocells may provide an important clue to the scenario of the emergence of primitive

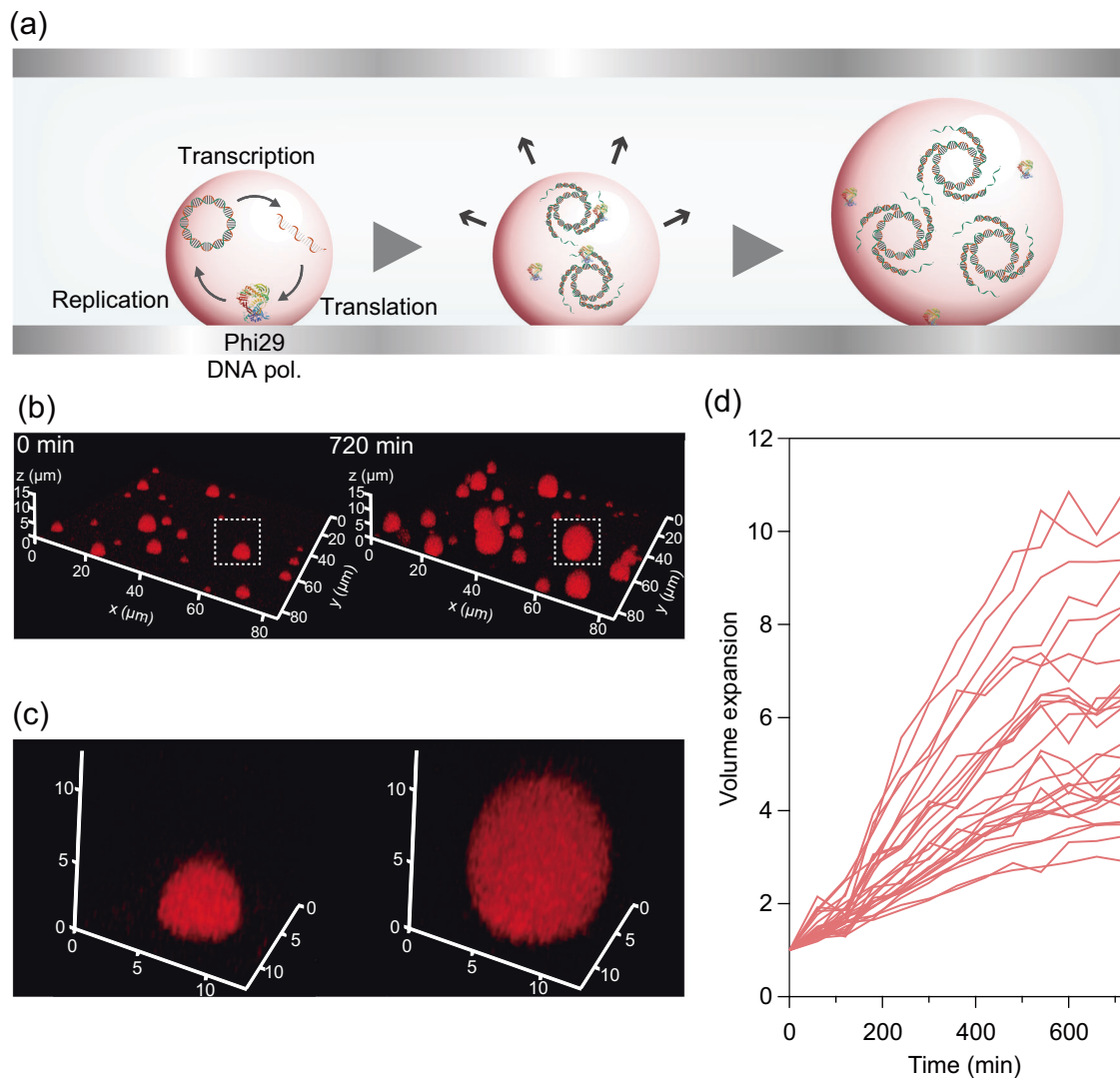


Fig. 6 | Self-growth by TXTL-coupled RCA. **a** Experimental diagram. Cell-free TXTL system (PURE system) was implemented to DEX droplet with DNA encoding EquiPhi29DNA tagged with dextran binding domain (EquiPhi29DNA-DBD). Upon the expression of EquiPhi29DNA-DBD and subsequent DNA amplification, the protocells showed the volume expansion. The image of phi29 DNA polymerase is obtained from PDB (PDB ID: 1XHX). **b** Confocal images of the protocell stained with

TRITC-DEX. Fluorescence images show the reaction at the start (0 min, left) and at 720 min (right). **c** Magnified droplet image surrounded by white dashed square in (b). **d** Time-courses of self-growth of the protocells. The volume was normalized with that at 0 min. These experiments were repeated more than three times with similar results, respectively.

life. However, it is crucial to examine other phase-separated systems for the further understanding of the potential mechanisms that could have driven the formation and evolution of early protocells.

Methods

Analysis of DNA partition ratio

The indicated mixtures of DNA (20 ng/ μ L), DEX, and PEG were prepared in 1.5 mL tubes and centrifuged at $20,000 \times g$ for 3 min. The mixture was separated into two layers: an upper layer rich in PEG and a lower layer rich in DEX. The DNA concentrations in each phase were determined from the fluorescence signal of SYBR Gold using calibration curves, each prepared for 10 bp, 100 bp, 4 kbp, or 205 kbp DNA in 4.0 w/w% DEX or 4.0 w/w% PEG (Supplementary Fig. 1).

Titrimetry of PEG/DEX ATPS with or without DNA

ATPS mixtures of the PEG/DEX system were prepared at the following concentrations: (1.2, 2.5), (2.3, 2.3), (3.2, 2.0), (4.8, 1.5), (6.0, 1.2), or (7.0, 0.9) with 4 kbp DNA (950 ng/ μ L), with 205 kbp DNA (950 ng/ μ L), or without DNA. 100 μ L of PEG/DEX mix was serially diluted by addition

of 2 μ L of pure water. Each time after the dilution, the samples were centrifuged at $20,000 \times g$ for 3 min for the segregation of PEG-rich layer on the top and DEX-rich layer at the bottom of tubes. To enhance the visual clarity of the phase separation, DEX- and PEG-rich phases were stained with 0.1 w/w% of TRITC-DEX and 0.1 w/w% of FITC-PEG.

Phase separation induced by RCA

RCA was conducted in PEG/DEX mix (2.00, 2.00) with a commercially available kit of EquiPhi29DNA in the presence of 8 pM circular 205 kbp DNA, 0.05 w/w% TRITC-DEX, 1 μ M SYTO 13, and 6 N random primer. The mixture was incubated at 33 $^{\circ}$ C for 16 h in a flow cell.

Self-growth induced by RCA

DEX-rich phase solution was prepared from the PEG/DEX mix (5.0, 5.0) containing 1x EquiPhi29TM DNA polymerase Reaction Buffer, 1 mM DTT, and 0.05 w/w% TRITC-DEX. PEG-rich phase solution was prepared from the PEG/DEX mix (2.5, 2.5) containing 1x EquiPhi29 DNA polymerase Reaction Buffer, 1 mM DTT, 1 mM each dNTPs, 10 μ M Exo-Resistant Random primer, 0.05 w/w% TRITC-DEX, 20 μ M SYTO 12 (only

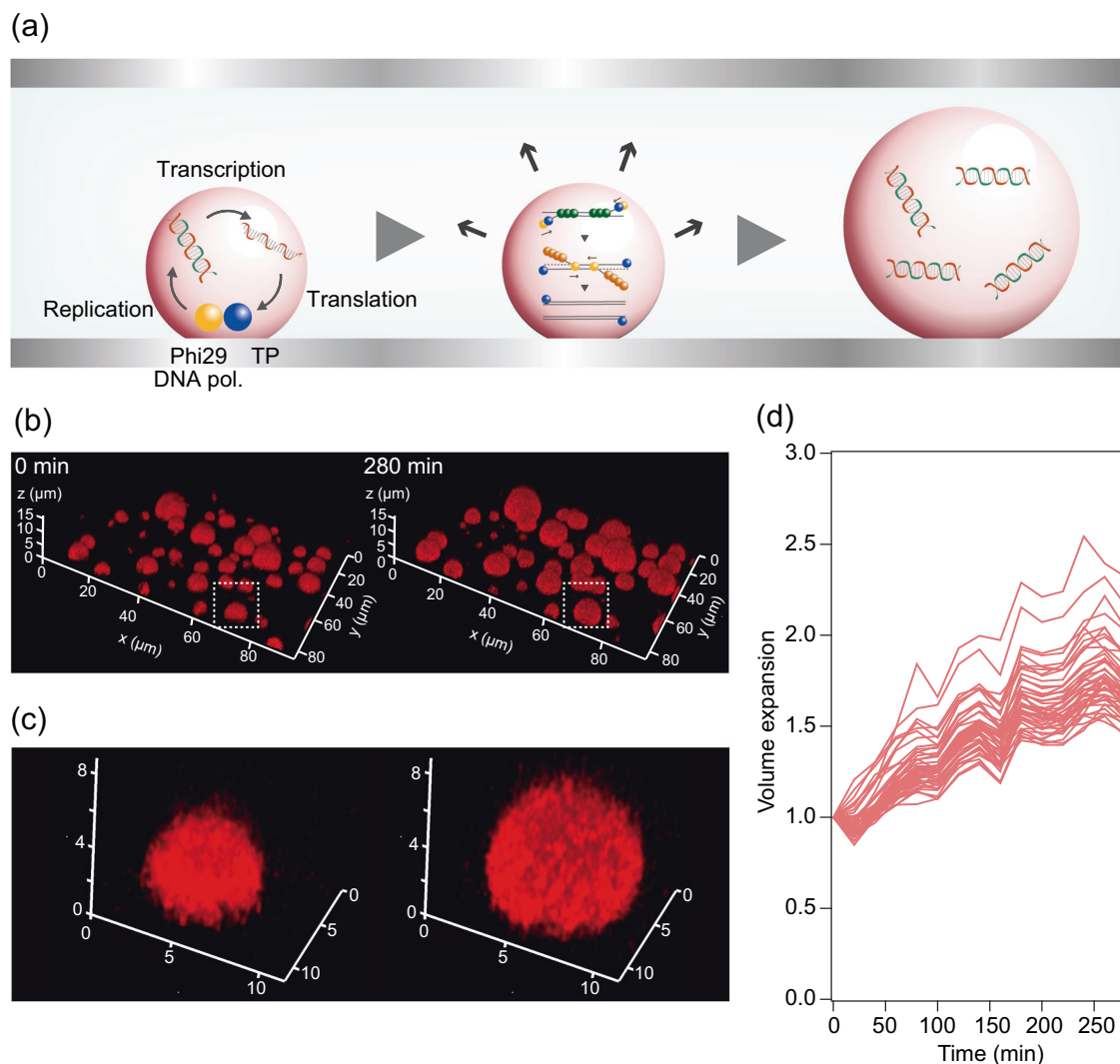


Fig. 7 | Self-growth by TXTL-coupled TPPDA. **a** Experimental diagram. Protocols containing TXTL system and terminal protein primed DNA amplification (TPPDA) system were incubated. The TXTL-coupled TPPDA system in this study was composed of template DNA encoding terminal protein and ϕ 29DNAP, and purified proteins: ssDNA binding protein (SSB) and dsDNA binding protein (DSB). **b** Confocal images of the protocell stained with TRITC-DEX. Fluorescence images

show the reaction at the start (0 min, left) and at 280 min (right). **c** Magnified images of DEX droplets surrounded by dashed square border in **(b)** at 0 min (left) and at 280 min (right). **d** The time-course of self-growth of protocells. The volume was normalized to that at 0 min. These experiments were repeated more than three times with similar results, respectively.

when monitoring the DNA concentration inside the DEX droplet). The sample was prepared by mixing 1 μ L DEX-rich phase solution, 50 μ L PEG-rich phase solution, 1 μ L 1.5 ng/ μ L 4.2 kbp plasmid DNA, and 2 μ L 1.5 μ M EquiPhi29 DNA polymerase. The flow cell, assembled from two CYTOP-coated coverslips, was preincubated with 1/10 diluted solution of solution B for TXTL kit (PURExpress, NEB) to make the bottom coverslip sticky and stably attach the droplet onto it. The solution was infused into a flow cell and incubated at 30 $^{\circ}$ C.

DNase I treatment on droplets after RCA

The PEG-rich phase solution was prepared from the PEG/DEX mixture (2.5, 2.5) containing 1x EquiPhi29 DNA polymerase reaction buffer, 1 mM DTT, 0.5 mM CaCl_2 , 0.03 w/w% TRITC-DEX. 8 μ L of PEG-rich phase solution was mixed with 1 μ L of 8 nM DNase I. After 3 h of droplet growth by RCA, the PEG solution surrounding the droplets was exchanged with the DNase I-containing solution.

Phase separation induced by spiked RNA

A plasmid DNA, pRSET B, encoding a derivative of mScarlet protein and eight Pepper sequences (8Pepper) downstream under T7

promoter, was used as the template. RNA transcript with 1750 nt long was synthesized with a ScriptMAX[®] Thermo T7 Transcription Kit and purified with NucleoSpin RNA Clean-up XS. The purified RNA was added at 623 ng/ μ L to the miscible PEG/DEX mixture (2.00, 2.00) with 0.05 w/w% TRITC-DEX and 20 μ M HBC.

Phase separation induced by in situ RNA transcription

A plasmid DNA, pRSET B, encoding a derivative of mScarlet protein and 8Pepper downstream under T7 promoter, was used as the template. The complete RNA transcript was ~1750 nt in length. 600 ng/ μ L of the template DNA and ScriptMAX[®] Thermo T7 Transcription Kit was added to miscible PEG/DEX mixture (2.00, 2.00) with 0.05 w/w% and HBC (20 μ M) and incubated at 33 $^{\circ}$ C for 16 h.

Self-growth by TXTL-coupled RCA

DEX-rich phase solution was prepared from the PEG/DEX mix (5.0, 5.0) containing solution A (PURExpress, NEB), 1x Energy mix and 0.01 w/w% TRITC-DEX. PEG-rich phase solution was prepared from the PEG/DEX mix (2.5, 2.5) containing 1x Energy mix, 1.2 mM each dNTPs, 10 μ M Exo-resistant primer, solution A at a ratio of 1/25 of the total volume, rNTP

mix at a ratio of 1/50 of the total volume, and 0.01 w/w% TRITC-DEX. The sample was composed of 1 μ L DEX-rich phase solution, 30 μ L PEG-rich phase solution, 1 μ L 60 ng/ μ L DNA encoding EquiPhi29 DNA polymerase tagged with DBD, and 3 μ L solution B. The flow cell, assembled from two CYTOP-coated coverslips, was preincubated with blocking solution containing 5 mg/mL BSA and 0.1 w/w% S386. The sample solution was infused into the flow cell assembled from two CYTOP-coated coverslips and incubated at 30 °C.

Self-growth by TXTL-coupled TPPDA

The 13 kbp linear DNA encoding ϕ 29DNAP, TP with phi29 origins was used as a template⁴⁴. DEX-rich phase solution was prepared from the PEG/DEX mix (8.0, 8.0) containing 20 mM ammonium sulfate, 1x Energy mix, 0.1 w/w% FITC-DEX. PEG-rich solution was prepared from the PEG/DEX mix (3.0, 3.0) containing 1x Energy mix, 20 mM ammonium sulfate, 1 mM dNTPs each, rNTP mix at a ratio of 1/50 of the total volume, solution A at a ratio of 1/25 of the total volume, 0.01 w/w% FITC-DEX. The sample was prepared by mixing 1 μ L DEX-rich phase solution and 30 μ L PEG-rich phase solution, 3 μ L 16.6 nM template DNA, 2.77 μ L 279 μ M DSB, 2.61 μ L 335 μ M SSB, 1.55 μ L 1.6 M NaCl, and 7.75 μ L solution B. The flow cell, assembled from two CYTOP-coated coverslips, was preincubated with blocking solution containing 5 mg/mL BSA and 0.1 w/w% S386. The solution was infused into a flow cell and incubated at 30 °C.

Preparation of DSB

With modifications, DSB was purified according to a previous report⁴². His6-TEV-DSB was expressed in *E. coli* Rosetta™ 2(DE3) pLysS Singles™ competent cells. Cell lysate was loaded onto a Ni-NTA column with loading buffer (50 mM Tris-HCl (pH 7.5), 7 mM β -mercaptoethanol, 0.5 mM EDTA, 5 w/w% glycerol, and 0.8 M NaCl). Elution was achieved using the elution buffer (50 mM Tris-HCl (pH 7.5), 0.5 mM EDTA, 7 mM β -mercaptoethanol, 5 w/w% glycerol, 0.2 M NaCl, and 500 mM imidazole). The eluted fraction was 1/10 diluted with Buffer A (50 mM Tris-HCl (pH 7.5), 7 mM β -mercaptoethanol, 1 mM EDTA, 5 w/w% glycerol) to reduce the NaCl concentration to 20 mM for loading to a Cytiva HiTrap™ Heparin HP column. After washing the column with Buffer A, His6-TEV-DSB was eluted using Buffer A with 0.4 M NaCl. Subsequently, the elute was 1/10 diluted with Buffer A and loaded onto a Cytiva HiTrap™ Q HP column. After washing the column with Buffer A, His6-TEV-DSB was eluted using Buffer A with 0.6 M NaCl. Intact DSB was obtained by the cleavage of His6-TEV tag using TEV protease (ProTEVPlus, Promega).

Preparation of SSB

With modifications, SSB was purified according to a previous report⁴⁸. SSB, fused with His6-tag, twin-strep-tag, and SUMO-tag at the N-terminus, was expressed in Rosetta™ 2(DE3)pLysS Singles™ competent cells. Cell lysate was loaded onto a streptactin column and washed with Buffer A with 0.8 M NaCl. Subsequently, SUMO protease solution (50 mM Tris-HCl (pH 7.5), 1 mM DTT, 1 mM EDTA, 20 nM SUMO protease, and 0.15 w/w% NP-40) was added to the resin, and SUMO-tag was cleaved by overnight incubation at 4 °C. After the recovery of intact SSB, it was loaded onto a Cytiva HiTrap™ Heparin HP column and eluted in the flowthrough. Following this, SSB was loaded onto a Cytiva HiTrap™ Q HP column. After washing the column with Buffer A, SSB was eluted using Buffer A with 0.1 M NaCl.

Microscopic imaging and image analysis

See Supplementary Information.

Reporting summary

Further information on research design is available in the Nature Portfolio Reporting Summary linked to this article.

Data availability

The data sets generated in this study are provided in the Supplementary Information/Source Data file. The original image data are available under restricted access for their large file size, access can be obtained by reasonable request from the corresponding author in a week. Source data file is available for Figs. 1, 2, 4–6 and supplementary figures. Supplementary videos are available for Figs. 3, 4, 6, 7 and S8. Source data are provided with this paper.

Code availability

Codes for data analysis are provided in supplementary files with this paper.

References

1. Spoelstra, W. K., Deshpande, S. & Dekker, C. Tailoring the appearance: what will synthetic cells look like? *Curr. Opin. Biotechnol.* **51**, 47–56 (2018).
2. Crowe, C. D. & Keating, C. D. Liquid-liquid phase separation in artificial cells. *Interface Focus* **8**, 20180032 (2018).
3. Ganzinger, K. A. & Schwille, P. More from less—bottom-up reconstitution of cell biology. *J. Cell Sci.* **132**, <https://doi.org/10.1242/jcs.227488> (2019).
4. Martin, N. Dynamic synthetic cells based on liquid-liquid phase separation. *ChemBioChem* **20**, 2553–2568 (2019).
5. Szostak, J. W., Bartel, D. P. & Luisi, P. L. Synthesizing life. *Nature* **409**, 387–390 (2001).
6. Tawfik, D. S. & Griffiths, A. D. Man-made cell-like compartments for molecular evolution. *Nat. Biotechnol.* **16**, 652–656 (1998).
7. Marshall, R. et al. Rapid and scalable characterization of CRISPR technologies using an *E. coli* cell-free transcription-translation system. *Mol. Cell* **69**, 146–157.e143 (2018).
8. Zhang, Y. et al. Accurate high-throughput screening based on digital protein synthesis in a massively parallel femtoliter droplet array. *Sci. Adv.* **5**, eaav8185 (2019).
9. Sato, W., Zajkowski, T., Moser, F. & Adamala, K. P. Synthetic cells in biomedical applications. *Wiley Interdiscip. Rev. Nanomed. Nanobiotechnol.* **14**, e1761 (2022).
10. Boyd, M. A. & Kamat, N. P. Designing artificial cells towards a new generation of biosensors. *Trends Biotechnol.* **39**, 927–939 (2021).
11. Ichihashi, N. et al. Darwinian evolution in a translation-coupled RNA replication system within a cell-like compartment. *Nat. Commun.* **4**, 2494 (2013).
12. Su'etsugu, M., Takada, H., Katayama, T. & Tsujimoto, H. Exponential propagation of large circular DNA by reconstitution of a chromosome-replication cycle. *Nucleic Acids Res.* **45**, 11525–11534 (2017).
13. Shimizu, Y., Kanamori, T. & Ueda, T. Protein synthesis by pure translation systems. *Methods* **36**, 299–304 (2005).
14. Bhattacharya, A., Brea, R. J., Niederholtmeyer, H. & Devaraj, N. K. A minimal biochemical route towards de novo formation of synthetic phospholipid membranes. *Nat. Commun.* **10**, 300 (2019).
15. Kuruma, Y., Stano, P., Ueda, T. & Luisi, P. L. A synthetic biology approach to the construction of membrane proteins in semi-synthetic minimal cells. *Biochim. Biophys. Acta* **1788**, 567–574 (2009).
16. Arumugam, S., Petrasek, Z. & Schwille, P. MinCDE exploits the dynamic nature of FtsZ filaments for its spatial regulation. *Proc. Natl. Acad. Sci. USA* **111**, E1192–E1200 (2014).
17. Eto, S. et al. Phospholipid synthesis inside phospholipid membrane vesicles. *Commun. Biol.* **5**, 1016 (2022).
18. Kohyama, S., Merino-Salomon, A. & Schwille, P. In vitro assembly, positioning and contraction of a division ring in minimal cells. *Nat. Commun.* **13**, 6098 (2022).

19. Zhu, T. F. & Szostak, J. W. Coupled growth and division of model protocell membranes. *J. Am. Chem. Soc.* **131**, 5705–5713 (2009).
20. Voegelé, K. et al. Towards synthetic cells using peptide-based reaction compartments. *Nat. Commun.* **9**, 3862 (2018).
21. Steinkühler, J. et al. Controlled division of cell-sized vesicles by low densities of membrane-bound proteins. *Nat. Commun.* **11**, 905 (2020).
22. Miele, Y. et al. Self-division of giant vesicles driven by an internal enzymatic reaction. *Chem. Sci.* **11**, 3228–3235 (2020).
23. Tsugane, M. & Suzuki, H. Elucidating the membrane dynamics and encapsulation mechanism of large DNA molecules under molecular crowding conditions using giant unilamellar vesicles. *ACS Synth. Biol.* **9**, 2819–2827 (2020).
24. Kurihara, K. et al. Self-reproduction of supramolecular giant vesicles combined with the amplification of encapsulated DNA. *Nat. Chem.* **3**, 775–781 (2011).
25. Blanken, D., Foschepoth, D., Serrao, A. C. & Danelon, C. Genetically controlled membrane synthesis in liposomes. *Nat. Commun.* **11**, 4317 (2020).
26. Sloodbeek, A. D., van Haren, M. H. I., Smokers, I. B. A. & Spruijt, E. Growth, replication and division enable evolution of coacervate protocells. *Chem. Commun.* **58**, 11183–11200 (2022).
27. Andre, A. A. M. & Spruijt, E. Liquid-liquid phase separation in crowded environments. *Int. J. Mol. Sci.* **21**, <https://doi.org/10.3390/ijms21165908> (2020).
28. Nakashima, K. K., van Haren, M. H. I., Andre, A. A. M., Robu, I. & Spruijt, E. Active coacervate droplets are protocells that grow and resist Ostwald ripening. *Nat. Commun.* **12**, 3819 (2021).
29. Deshpande, S. et al. Spatiotemporal control of coacervate formation within liposomes. *Nat. Commun.* **10**, 1800 (2019).
30. Spoelstra, W. K., van der Sluis, E. O., Dogterom, M. & Reese, L. Nonspherical coacervate shapes in an enzyme-driven active system. *Langmuir* **36**, 1956–1964 (2020).
31. Monterroso, B., Zorrilla, S., Sobrinos-Sanguino, M., Keating, C. D. & Rivas, G. Microenvironments created by liquid-liquid phase transition control the dynamic distribution of bacterial division FtsZ protein. *Sci. Rep.* **6**, 35140 (2016).
32. Sobrinos-Sanguino, M., Zorrilla, S., Keating, C. D., Monterroso, B. & Rivas, G. Encapsulation of a compartmentalized cytoplasm mimic within a lipid membrane by microfluidics. *Chem. Commun.* **53**, 4775–4778 (2017).
33. Nakatani, N. et al. Specific spatial localization of actin and DNA in a water/water microdroplet: self-emergence of a cell-like structure. *ChemBioChem* **19**, 1370–1374 (2018).
34. Torre, P., Keating, C. D. & Mansy, S. S. Multiphase water-in-oil emulsion droplets for cell-free transcription-translation. *Langmuir* **30**, 5695–5699 (2014).
35. Strulson, C. A., Molden, R. C., Keating, C. D. & Bevilacqua, P. C. RNA catalysis through compartmentalization. *Nat. Chem.* **4**, 941–946 (2012).
36. Mizuuchi, R. & Ichihashi, N. Translation-coupled RNA replication and parasitic replicators in membrane-free compartments. *Chem. Commun.* **56**, 13453–13456 (2020).
37. Hatti-Kaul, R. *Aqueous Two-Phase Systems: Methods and Protocols* (Springer, 2000).
38. Povilaitis, T., Alzbutas, G., Sukackaitė, R., Siurkus, J. & Skirgaila, R. In vitro evolution of phi29 DNA polymerase using isothermal compartmentalized self replication technique. *Protein Eng. Des. Sel.* **29**, 617–628 (2016).
39. Libicher, K., Hornberger, R., Heymann, M. & Mutschler, H. In vitro self-replication and multicistronic expression of large synthetic genomes. *Nat. Commun.* **11**, 904 (2020).
40. Shimizu, Y. et al. Cell-free translation reconstituted with purified components. *Nat. Biotechnol.* **19**, 751–755 (2001).
41. Minagawa, Y., Nakata, S., Date, M., Li, Y. & Noji, H. On-chip enrichment system for digital bioassay based on aqueous two-phase system. *ACS Nano* **17**, 212–220 (2023).
42. Mencia, M., Gella, P., Camacho, A., de Vega, M. & Salas, M. Terminal protein-primed amplification of heterologous DNA with a minimal replication system based on phage Phi29. *Proc. Natl. Acad. Sci. USA* **108**, 18655–18660 (2011).
43. Sakatani, Y., Yomo, T. & Ichihashi, N. Self-replication of circular DNA by a self-encoded DNA polymerase through rolling-circle replication and recombination. *Sci. Rep.* **8**, 13089 (2018).
44. van Nies, P. et al. Self-replication of DNA by its encoded proteins in liposome-based synthetic cells. *Nat. Commun.* **9**, 1583 (2018).
45. Kurisu, M. et al. Synthesising a minimal cell with artificial metabolic pathways. *Commun. Chem.* **6**, 56 (2023).
46. Frank, T., Voegelé, K., Dupin, A., Simmel, F. C. & Pirzer, T. Growth of giant peptide vesicles driven by compartmentalized transcription-translation activity. *Chem. Eur. J.* **26**, 17356–17360 (2020).
47. Sato, Y., Sakamoto, T. & Takinoue, M. Sequence-based engineering of dynamic functions of micrometer-sized DNA droplets. *Sci. Adv.* **6**, eaba3471 (2020).
48. Soengas, M. S., Gutierrez, C. & Salas, M. Helix-destabilizing activity of phi 29 single-stranded DNA binding protein: effect on the elongation rate during strand displacement DNA replication. *J. Mol. Biol.* **253**, 517–529 (1995).

Acknowledgements

We thank Ryoko Yaginuma for technical support. We also thank Yuki Goto from Kyoto University and Kazuhito V. Tabata from The University of Tokyo for generously providing the HBC reagent. This work was financially supported by CREST, Japan (JPMJCR19S4 to H.N. and JPMJCR18S6 to M.S.) from Japan Science and Technology Agency (JST), GteX program (JPMJGX23B1 to H.N.) from JST, ASPIRE (JPMJAP24B5 to H.N.) from JST, Grant-in-Aids for Scientific Research (S) (JP19H05624 to H.N.) from Japan Society for the Promotion of Science (JSPS) and Grant-in-Aid for Research Fellows (22J22681 to M.Y.) from JSPS.

Author contributions

H.N. conceived the idea of the research and supervised it. Y.M. designed the experiments. Y.M. and M.Y. conducted the experiments and analyzed the data. M.S. provided technical support. H.N., Y.M., and M.Y. wrote the manuscript.

Competing interests

The authors declare no competing interests.

Additional information

Supplementary information The online version contains supplementary material available at <https://doi.org/10.1038/s41467-025-56172-7>.

Correspondence and requests for materials should be addressed to Hiroyuki Noji.

Peer review information *Nature Communications* thanks the anonymous reviewers for their contribution to the peer review of this work. A peer review file is available.

Reprints and permissions information is available at <http://www.nature.com/reprints>

Publisher's note Springer Nature remains neutral with regard to jurisdictional claims in published maps and institutional affiliations.

Open Access This article is licensed under a Creative Commons Attribution-NonCommercial-NoDerivatives 4.0 International License, which permits any non-commercial use, sharing, distribution and reproduction in any medium or format, as long as you give appropriate credit to the original author(s) and the source, provide a link to the Creative Commons licence, and indicate if you modified the licensed material. You do not have permission under this licence to share adapted material derived from this article or parts of it. The images or other third party material in this article are included in the article's Creative Commons licence, unless indicated otherwise in a credit line to the material. If material is not included in the article's Creative Commons licence and your intended use is not permitted by statutory regulation or exceeds the permitted use, you will need to obtain permission directly from the copyright holder. To view a copy of this licence, visit <http://creativecommons.org/licenses/by-nc-nd/4.0/>.

© The Author(s) 2025